



GDF15 activates AMPK and inhibits gluconeogenesis and fibrosis in the liver by attenuating the TGF- β 1/SMAD3 pathway

Javier Jurado-Aguilar^{a,b,c,d,1}, Emma Barroso^{a,b,c,d,1}, Maribel Bernard^{a,b,c,d},
Meijian Zhang^{a,b,c,d}, Mona Peyman^{a,b,c,d}, Patricia Rada^{c,e}, Ángela M. Valverde^{c,e},
Walter Wahli^{f,g,h}, Xavier Palomer^{a,b,c,d}, Manuel Vázquez-Carrera^{a,b,c,d,*}

^a Department of Pharmacology, Toxicology and Therapeutic Chemistry, Faculty of Pharmacy and Food Sciences, Spain

^b Institute of Biomedicine of the University of Barcelona (IBUB), University of Barcelona, 08028 Barcelona, Spain

^c Spanish Biomedical Research Center in Diabetes and Associated Metabolic Diseases (CIBERDEM)-Instituto de Salud Carlos III, 28029 Madrid, Spain

^d Pediatric Research Institute-Hospital Sant Joan de Déu, 08950 Esplugues de Llobregat, Spain

^e Instituto de Investigaciones Biomédicas Alberto Sols (CSIC/UAM), Madrid, Spain

^f Center for Integrative Genomics, University of Lausanne, CH-1015 Lausanne, Switzerland

^g Lee Kong Chian School of Medicine, Nanyang Technological University Singapore, Singapore 308232

^h ToxAlim (Research Center in Food Toxicology), INRAE, UMR1331, F-31300 Toulouse Cedex, France

ARTICLE INFO

Keywords:

GDF15
AMPK
SMAD3
TGF- β
Gluconeogenesis
Fibrosis

ABSTRACT

Introduction: The levels of the cellular energy sensor AMP-activated protein kinase (AMPK) have been reported to be decreased via unknown mechanisms in the liver of mice deficient in growth differentiation factor 15 (GDF15). This stress response cytokine regulates energy metabolism mainly by reducing food intake through its hindbrain receptor GFRAL.

Objective: To examine how GDF15 regulates AMPK.

Methods: Wild-type and *Gdf15*^{-/-} mice, mouse primary hepatocytes and the human hepatic cell line Huh-7 were used.

Results: *Gdf15*^{-/-} mice showed glucose intolerance, reduced hepatic phosphorylated AMPK levels, increased levels of phosphorylated mothers against decapentaplegic homolog 3 (SMAD3; a mediator of the fibrotic response), elevated serum levels of transforming growth factor (TGF)- β 1, as well as upregulated gluconeogenesis and fibrosis. In line with these observations, recombinant (r)GDF15 promoted AMPK activation and reduced the levels of phosphorylated SMAD3 and the markers of gluconeogenesis and fibrosis in the liver of mice and in mouse primary hepatocytes, suggesting that these effects may be independent of GFRAL. Pharmacological inhibition of SMAD3 phosphorylation in *Gdf15*^{-/-} mice prevented glucose intolerance, the deactivation of AMPK and the increase in the levels of proteins involved in gluconeogenesis and fibrosis, suggesting that overactivation of the TGF- β 1/SMAD3 pathway is responsible for the metabolic alterations in *Gdf15*^{-/-} mice.

Conclusions: Overall, these findings indicate that GDF15 activates AMPK and inhibits gluconeogenesis and fibrosis by lowering the activity of the TGF- β 1/SMAD3 pathway.

1. Introduction

Growth differentiation factor 15 [GDF15; also known as macrophage inhibitory cytokine 1, nonsteroidal anti-inflammatory drug activated gene-1, or placental bone morphogenetic protein] is a cytokine regarded as a divergent member of the transforming growth factor β (TGF- β) superfamily whose levels are remarkably elevated under conditions of

cellular stress. Therefore, GDF15 has been widely used as a biomarker for the severity of several pathologies [1]. In addition, GDF15 regulates the energy balance by reducing food intake. The anorectic effect of GDF15 is mediated by its binding to its cognate receptor, glial cell line-derived neurotrophic factor (GDNF) family receptor α -like (GFRAL) [2–5]. This receptor is expressed solely in the neurons of the area postrema and the nucleus of the solitary tract [5], which are important

* Corresponding author at: Unitat de Farmacologia, Facultat de Farmàcia i Ciències de l'Alimentació, Av. Joan XXIII 27-31, E-08028 Barcelona, Spain.

E-mail address: mvazquezcarrera@ub.edu (M. Vázquez-Carrera).

¹ Both authors contributed equally.

brain regions involved in appetite and weight regulation. Consistent with a role for GDF15 in appetite regulation, the administration of recombinant (r)GDF15 reduces food intake and body weight in wild-type (WT) mice, but not in *Gdf15*-knockout mice [2,4,5]. Likewise, transgenic mice overexpressing *Gdf15* are characterized by a lower food intake and are more resistant to obesity and glucose intolerance [6–9]. However, obese mice and humans show increased levels of circulating GDF15, suggesting a resistance to the effects of this cytokine [10]. Interestingly, a recent study has provided a mechanism for GDF15 resistance in obesity involving the membrane-bound matrix metalloproteinase 14 (MMP14 or MT1-MMP). Activation of MT1-MMP in obese rodents leads to the proteolytic inactivation of GFRAL [11], thereby mitigating the anorectic effect of GDF15.

Although many of the effects of GDF15 on energy metabolism can be attributed to the reduction of appetite and body weight mediated via the central receptor GFRAL, several recent studies have reported that GDF15 also exerts peripheral effects independently of GFRAL [12,13]. Regarding energy metabolism, our group has previously reported that GDF15 activates the cellular energy sensor AMP-activated protein kinase (AMPK) in cultured myotubes and isolated skeletal muscle that do not express GFRAL [14]. However, how GDF15 regulates AMPK phosphorylation has remained unknown. In this work, we describe that *Gdf15*-deficient mice show glucose intolerance and reduced hepatic phosphorylated AMPK levels that are accompanied by increases in hepatic gluconeogenesis and fibrosis. These changes are mediated by an increase in the serum levels of TGF- β 1 and in the hepatic phosphorylated levels of mothers against decapentaplegic homolog 3 (SMAD3), a mediator of the fibrotic response. In addition, rGDF15 activates AMPK and reduces phosphorylated SMAD3 levels in the liver of mice as well as in mouse primary hepatocytes, suggesting that these effects are not mediated by GFRAL. Overall, these findings indicate that GDF15 activates AMPK and inhibits hepatic gluconeogenesis and fibrosis by attenuating the TGF- β 1/SMAD3 pathway.

2. Materials and methods

2.1. Animals and treatments

Male and female *Gdf15*^{-/-} [15] and wild-type (WT) littermates (10–12 weeks old) mice, provided by Dr. Se-Jin Lee (Johns Hopkins University School of Medicine, USA), were maintained in 12-h light/dark cycle, temperature (22 °C) and humidity-controlled rooms, and fed *ad libitum* with standard diet with free access to water. After sacrifice, liver samples were frozen in liquid nitrogen before being stored at –80 °C.

To treat the animals with exogenous rGDF15, male C57BL/6 mice (10–12 weeks old) (Envigo, Barcelona, Spain) were randomly distributed into two experimental groups ($n = 5$ each). At 8 AM, one of the groups received a single subcutaneous injection of saline, while the other received a single subcutaneous injection of rGDF15 (catalog 8944-GD, R&D Systems, Minneapolis, MN, USA) (0.1 mg/kg). The mice were sacrificed four hours later at noon. In a second treatment, male C57BL/6 mice (10–12 weeks old) were randomly distributed into two experimental groups ($n = 5$ each). Animals were fasted overnight and at 8 AM, one of the groups received a single subcutaneous injection of saline, while the other received a single subcutaneous injection of rGDF15 (0.1 mg/kg). The mice were sacrificed four hours later, and liver samples were frozen in liquid nitrogen before being stored at –80 °C. These samples were used to determine the levels of phosphorylated AMPK and gluconeogenic proteins.

To inhibit SMAD3 *in vivo*, male *Gdf15*^{-/-} and WT mice (10–12 weeks old) were randomly distributed into three experimental groups: WT mice and one group of *Gdf15*^{-/-} mice were treated with vehicle, and the second group of *Gdf15*^{-/-} with the specific inhibitor of SMAD3 phosphorylation, SIS3 (S0447 Sigma-Aldrich, St. Louis, MO, USA) (2 mg/kg/day in 5 % dimethyl sulfoxide diluted in serum, i.p.) [16]. At the

end of the 7-day treatment, mice were sacrificed, and liver samples were frozen in liquid nitrogen before being stored at –80 °C.

For the glucose tolerance test (GTT), male and female mice fasted for 6 h received 2 g/kg of body weight of glucose through an i.p. injection and blood was collected from the tail vein after 0, 15, 30, 60 and 120 min for glucose determination. In the pyruvate tolerance test (PTT), male and female mice fasted for 15 h received 2 g/kg of body weight of sodium pyruvate (Sigma-Aldrich, P2256) through an i.p. injection and blood was collected from the tail vein at different time points for glucose determination.

Alanine aminotransferase (ALT) and aspartate aminotransferase (AST) activities in plasma samples were determined using the ALT/GPT and AST/GOT Spinreact kits (Spinreact, Girona, Spain), based on the spectrophotometric measurement of the rate of reduction in NADH levels.

The animal experiments complied with the Guide for the Care and Use of Laboratory Animals published by the US National Institutes of Health (8th edition: National Academies Press; 2011). All procedures were approved by the Bioethics Committee of the University of Barcelona, as stated in Law 5/21 July 1995 passed by the Generalitat de Catalunya. The animals were treated humanely and all efforts were made to minimize both animal numbers and suffering.

2.2. Liver histology

For histological staining studies, 4- μ m tissue sections obtained from formalin-fixed paraffin-embedded samples were stained with hematoxylin and eosin (H&E) to assess liver histology. Sirius red and Masson's trichrome staining were conducted to assess fibrosis. Sirius red, Masson's trichrome and Oil Red O (ORO) staining (Sigma-Aldrich) was performed on frozen 10- μ m liver sections. Twelve images at a magnification of 20 \times were captured to quantify the red-stained collagen or lipid droplets, with the red-stained area evaluated per total area using ImageJ.

2.3. Liver triglyceride content

Liver triglycerides were extracted according to Bligh & Dyer [17]. The lipid extract was evaporated under a stream of nitrogen gas, redissolved in absolute ethanol, and quantified using a commercial kit (Spinreact SA, St. Esteve de Bas, Spain).

2.4. Cell culture

Human Huh-7 hepatoma cells (kindly donated by Dr. Mayka Sanchez from the Josep Carreras Leukemia Research Institute, Barcelona, Spain) were cultured in DMEM supplemented with 10 % fetal bovine serum and 1 % penicillin-streptomycin at 37 °C under 5 % CO₂. For SMAD3 phosphorylation inhibition, the Huh-7 cells were incubated with 10 μ M SIS3 for 24 h.

Mouse primary hepatocytes were isolated from non-fasting male C57BL/6 or male *Gdf15*^{-/-} and WT mice (10–12 weeks old) by perfusion with collagenase, as described elsewhere [18]. The following day, hepatocytes were incubated in serum-free DMEM supplemented with 5.5 mM glucose in either the absence (control cells) or presence of *E. coli*-derived mouse rGDF15 protein (100 or 500 ng/mL) for 24 h (R&D Systems, catalog 8944-GD).

Glucose production in primary hepatocytes was measured using the glucose oxidase-peroxidase method (Biosystems, Spain). Briefly, 24 h after plating, primary hepatocytes were cultured in serum-free, phenol-free DMEM medium with 5.5 mM glucose and 1 mM glutamine for 3 h. Then, cells were washed twice with glucose production medium (DMEM without glucose and phenol red, 1 mM glutamine, 2 mM sodium pyruvate, 20 mM sodium lactate) to remove glucose from the culture plates and incubated in this medium for 16 h. At the end of the culture time, glucose was measured by the glucose oxidase-peroxidase method

according to the assay manufacturer's instructions. Glucose levels were referred to total protein content of each culture plate.

Lipid accumulation in primary hepatocytes incubated in the presence or absence of fatty acid-free bovine serum albumin (BSA) or BSA conjugated with palmitic acid was conducted by staining the cells with ORO. After complete washing and drying, 100 % isopropanol was added to each well and incubated on a shaker for 10 min at room temperature to release the ORO from the stained cells. Finally, 50 μ L of the ORO-containing extract was transferred to a 96-well plate, and the absorbance at a wavelength of 518 nm was measured with a microplate reader.

2.5. Reverse transcription-polymerase chain reaction and quantitative polymerase chain reaction

Isolated RNA was reverse transcribed to obtain 1 μ g of complementary DNA (cDNA), using Random Hexamers (Thermo Scientific), 10 mM deoxynucleotide (dNTP) mix and the reverse transcriptase enzyme derived from the Moloney murine leukemia virus (MMLV, Thermo Fisher, Waltham, MA, USA). The experiment was run in a thermocycler (Bio-Rad, Hercules, CA, USA) and consisted of a program with different steps and temperatures: 65 $^{\circ}$ C for 5 min, 4 $^{\circ}$ C for 5 min, 37 $^{\circ}$ C for 2 min, 25 $^{\circ}$ C for 10 min, 37 $^{\circ}$ C for 50 min, and 70 $^{\circ}$ C for 15 min. The relative levels of specific mRNAs were assessed by real-time RT-PCR in a Mini 48-Well T100™ thermal cycler (Bio-Rad), using the SYBR Green Master Mix (Applied Biosystems, Waltham, MA, USA), as previously described [14]. Briefly, samples had a final volume of 20 μ L, with 20 ng of total cDNA, 0.9 μ M of the primer mix, and 10 μ L of 2 \times SYBR Green Master Mix. The thermal cycler protocol for real-time PCR included the first step of denaturation at 95 $^{\circ}$ C for 10 min followed by 40 repeated cycles of 95 $^{\circ}$ C for 15 s, 60 $^{\circ}$ C for 30 s, and 72 $^{\circ}$ C for 30 s for denaturation, primer annealing, and amplification, respectively. Primer sequences were designed using the Primer-BLAST tool (NCBI), based on the full mRNA sequences to find the optimal primers for amplification, and evaluated with the Oligo-Analyzer Tool (Integrated DNA Technologies) to ensure an optimal melting temperature (T_m) and avoid the formation of homo/heterodimers or non-specific structures that can affect the interpretation of the results. The primer sequences were designed specifically to span the junction between the exons. The primer sequences used are provided in Supplementary Table 1. Values were normalized to the expression levels of glyceraldehyde 3-phosphate dehydrogenase (*Gapdh*) and measurements were performed in duplicate. All the changes in expression were normalized to the untreated control.

2.6. Immunoblotting

The isolation of total protein extracts was performed as described elsewhere [19]. Immunoblotting was performed with antibodies against ACC (#3662, Cell Signaling Technology, Danvers, MA, USA), phosphorylated (p)ACC^{S79} (#3661, Cell Signaling Technology), AMPK (#2532, Cell Signaling Technology), pAMPK^{T172} (#2531, Cell Signaling Technology), β -actin (A5441, Sigma), CRT2 (ab184239, Abcam, Cambridge, UK), pCRT2^{S171} (ab203187, Abcam), CHOP (GTX112827, Genetex, Irvine, CA, USA), GAPDH (MAB374, Millipore, Burlington, MA, USA), FASN (#610962, BD Biosciences, San Jose, CA, USA), G6Pase (BS-13386R, Bioss, Woburn, MA, USA), NF- κ B p65 (sc-109, Santa Cruz Biotechnology Inc., Dallas, TX, USA), PAI-1 (#11907, Cell Signaling Technology), PEPCK (sc-271029, Santa Cruz Biotechnology Inc.), PP2A (#2259, Cell Signaling Technology), α -SMA (A2547, Sigma), SMAD3 (#9513, Cell Signaling Technology) and pSMAD3^{S425} (sc-517575, Santa Cruz Biotechnology Inc.). Signal acquisition was performed using the Amersham Imager 680 apparatus and quantification of the immunoblot signal was performed with the Bio-Rad Image Lab software. The protein quantification results were normalized to the levels of a control protein to avoid unwanted sources of variation.

2.7. Determination of malonyl-CoA levels

Hepatic concentrations of malonyl-CoA were measured by an enzyme-linked immunosorbent assay (ELISA) (CSB-E12896m; Cusabio, Houston, TX, USA).

2.8. TGF- β 1 measurements

TGF- β 1 levels were measured in mouse liver homogenates and serum using an R&D Systems Quantikine ELISA kit, following the manufacturer's instructions.

2.9. Statistical analysis

Results are expressed as the mean \pm SEM. Significant differences were assessed by either Student's *t*-test or one-way and two-way ANOVA, according to the number of groups compared, using the GraphPad Prism program (version 9.0.2) (GraphPad Software Inc., San Diego, CA, USA). When significant variations were found by ANOVA, Tukey's post-hoc test for multiple comparisons was performed only if *F* achieved a *p* value <0.05. Differences were considered significant at *p* < 0.05.

3. Results

3.1. *Gdf15*^{-/-} mice display glucose intolerance and increased gluconeogenesis

First, we assessed abnormalities in glucose homeostasis in mice deficient in *Gdf15* by conducting a glucose tolerance test (GTT). Male *Gdf15*^{-/-} mice showed glucose intolerance when compared to WT mice (Fig. 1A-B). Similarly, female *Gdf15*^{-/-} mice also showed glucose intolerance (Supplementary Fig. 1A-B), and no differences were observed between the male and female mice, indicating an absence of sex differences regarding glucose handling in the mutant mice. The changes in glucose tolerance in male mice were observed in the absence of significant differences in body weight (Supplementary Fig. 1C) and food intake (Supplementary Fig. 1D) between the WT and *Gdf15*^{-/-} mice. Moreover, in agreement with our previous studies [14], a reduction in the hepatic levels of AMPK phosphorylated at Thr¹⁷² was observed in the *Gdf15*^{-/-} mice (Fig. 1C). Phosphorylation of this residue within the α subunit is required for AMPK activation and is achieved by liver kinase B1 (LKB1) and Ca²⁺/calmodulin-dependent protein kinase- β (CaMKK β) [20]. There was no difference in the phosphorylated levels of LKB1 and CaMKK β between the *Gdf15*^{-/-} and WT mice (Fig. 1D), suggesting that these kinases were not involved in the regulation of AMPK phosphorylation by GDF15. AMPK is inhibited through Thr¹⁷² dephosphorylation by protein phosphatases such as protein phosphatase 2 A (PP2A). Remarkably, the levels of PP2A were elevated in the livers of *Gdf15*^{-/-} mice (Fig. 1D), indicating a potential mechanism for the reduction of phosphorylated AMPK levels in these mice. Next, we tested whether the reduction in phosphorylated AMPK levels in the liver of *Gdf15*^{-/-} mice had an effect on its activity by evaluating several of its target pathways. It is well known that AMPK inhibits hepatic gluconeogenesis [20]. On the contrary, this process is stimulated by the phosphorylation of cAMP response element-binding protein (CREB), which, together with CREB regulated transcription coactivator 2 (CRT2, also referred to as transducer of regulated CREB activity 2, TORC2), drives the expression of peroxisome proliferator-activated receptor γ coactivator 1 α (PGC-1 α). This coactivator associates with several transcription factors to induce the expression of key genes encoding the gluconeogenic enzymes phosphoenolpyruvate carboxykinase (PEPCK) and glucose-6-phosphatase (G6Pase). AMPK inhibits gluconeogenesis by phosphorylating and reducing the nuclear translocation of CRT2 [21,22]. Consistent with the reduction in phosphorylated AMPK levels, the phosphorylated levels of CRT2 were reduced

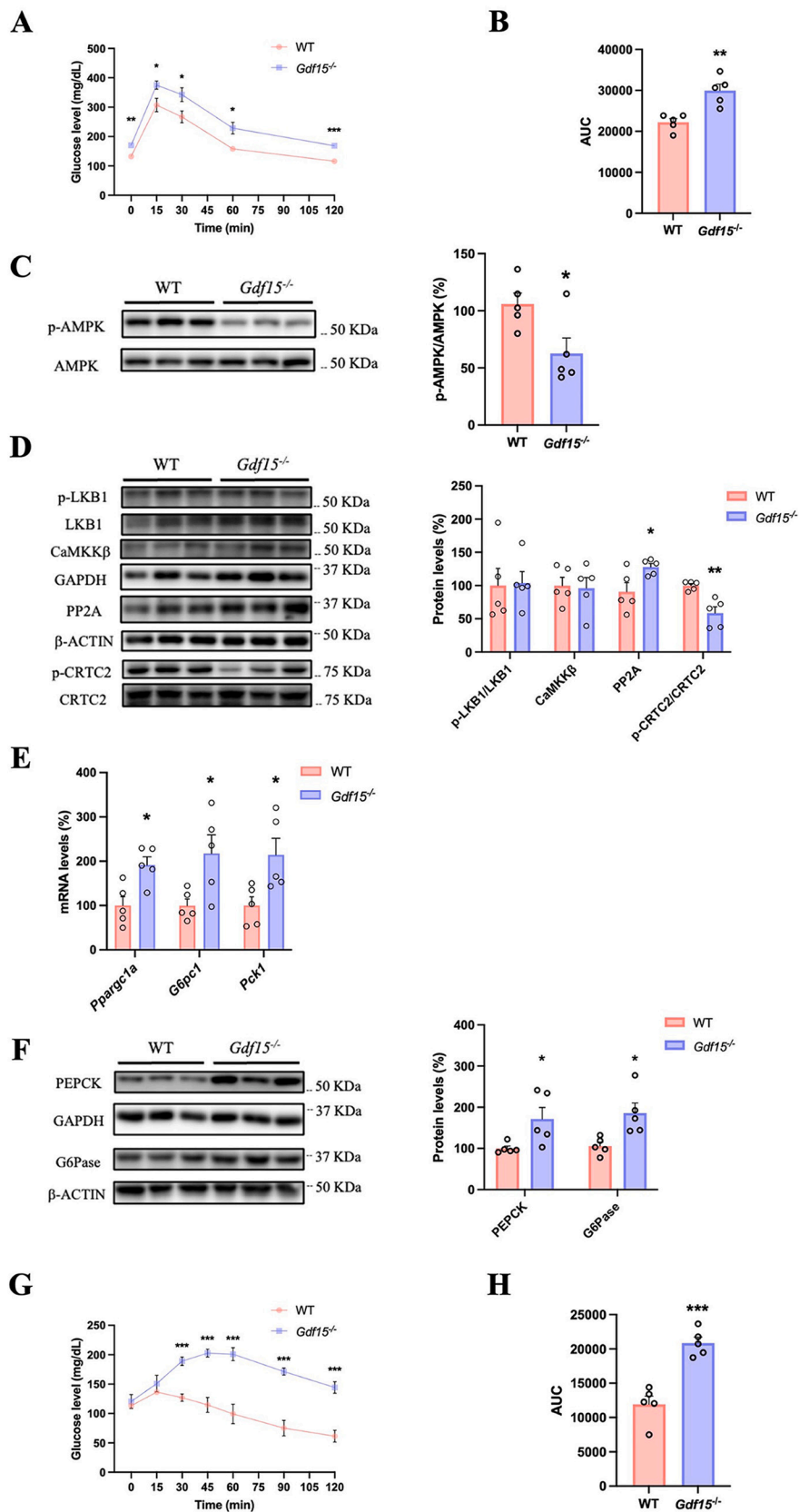


Fig. 1. *Gdf15*^{-/-} mice exhibit glucose intolerance and increased gluconeogenesis.

(A) Glucose tolerance test (GTT) and (B) area under the curve (AUC) in male wild-type (WT) and *Gdf15*^{-/-} mice fed a standard diet. (C) Immunoblot analysis of total and phosphorylated AMPK in the liver of WT and *Gdf15*^{-/-} mice. (D) Immunoblot analysis of total and phosphorylated LKB1, CaMKKβ, PP2A, and total and phosphorylated CRT2 in the liver of WT and *Gdf15*^{-/-} mice. (E) Hepatic mRNA levels of *Ppargc1a*, *G6pc1* and *Pck1*. (F) Immunoblot analysis of PEPCCK and G6Pase.

(G) Pyruvate tolerance test (PTT) and (H) area under the curve (AUC) in WT and *Gdf15*^{-/-} mice. *n* = 5 per group. Data are presented as the mean ± SEM. Significant differences were established by Student's *t*-test. **p* < 0.05, ***p* < 0.01 and ****p* < 0.001 vs. WT.

(Fig. 1D) and the expression levels of *Ppargc1a*, *G6pc1* and *Pck1* were increased (Fig. 1E) in the liver of *Gdf15*^{-/-} mice. In accordance with the mRNA expression levels, the protein amounts of PEPCK and G6Pase were higher in the *Gdf15*^{-/-} mice than in the WT animals (Fig. 1F). These findings suggest that GDF15 deficiency promotes gluconeogenesis. To validate this proposition, we conducted a pyruvate tolerance test (PTT) to estimate the level of hepatic gluconeogenesis. Interestingly, male *Gdf15*^{-/-} mice exhibited a significant increase in hepatic glucose production in comparison with the WT animals (Fig. 1G-H). No significant differences were observed between the males and females in the PTT (Supplementary Fig. 1E-F). Overall, these findings indicate that gluconeogenesis is increased in the *Gdf15*^{-/-} mice through a mechanism that might involve a reduction in AMPK activity.

3.2. Increased steatosis and fibrosis in the livers of *Gdf15*^{-/-} mice

H&E and ORO staining showed significant hepatic lipid accumulation in the *Gdf15*^{-/-} mice (Fig. 2A), that was confirmed by quantification of the accumulation of triglycerides in the liver (Fig. 2B). We then assessed if hepatic steatosis in the *Gdf15*^{-/-} mice correlated with the reduced activity of AMPK, since this kinase regulates lipid metabolism through the phosphorylation of its downstream target acetyl-CoA carboxylase (ACC). Phosphorylated ACC inhibits the production of malonyl-CoA, a substrate for fatty acid synthase (FASN) and a precursor for the *de novo* synthesis of palmitate, which is then converted into monounsaturated fatty acids by the activity of stearoyl-CoA desaturase 1 (SCD1). These fatty acids are ultimately accumulated as triglycerides by the activity of glycerol-3-phosphate acyltransferase (GPAT) (see scheme in Fig. 10). In line with the reduction in phosphorylated AMPK levels, *Gdf15*^{-/-} mice displayed a reduction in phosphorylated ACC and an increase in malonyl-CoA, while the hepatic expression of *Scd1*, *Fasn* and *Gpat* was induced (Fig. 2C-E). Consistent with the elevation in *Fasn* expression, FASN protein levels were increased in the liver of *Gdf15*^{-/-} mice (Fig. 2F). Collectively, these findings suggest that the reduction in AMPK activity caused by *Gdf15* deficiency contributes to hepatic steatosis by the stimulation of lipogenesis.

Further examination of the *Gdf15*^{-/-} mice showed that the serum levels of alanine aminotransferase (ALT) and aspartate aminotransferase (AST), two markers of liver injury, were increased compared to the WT animals (Fig. 3A and B). Endoplasmic reticulum (ER) stress and inflammation are important triggers for fibrosis [23]. The livers of *Gdf15*^{-/-} mice showed increased expression of the ER stress marker C/EBP homologous protein [*Chop*; or DNA damage-inducible transcript 3 (*Ddit3*)], but not of the binding immunoglobulin protein/78-kDa glucose-regulated protein (*BiP/Grp78*), whereas the expression levels of the pro-inflammatory markers interleukin 1 β (*Il1b*) and tumor necrosis factor α (*Tnfa*) were upregulated, although that of *Il6* was not (Fig. 3C). Similarly, macrophage infiltration contributes to fibrosis. In this sense, the mRNA levels of monocyte chemoattractant protein-1 [*Mcp1*; or chemokine (C-C motif) ligand 2 (*Ccl2*)], responsible for attracting monocytes and T cells during liver injury, and of the macrophage marker F4/80 (*Adgre1*) were significantly upregulated in the livers of *Gdf15*^{-/-} mice (Fig. 3C). Moreover, the expression of the anti-inflammatory M2 macrophage gene markers *Arg1* and *Il10* was reduced in the livers of *Gdf15*^{-/-} mice (Fig. 3C). This finding, together with the increase in the levels of M1 macrophage gene markers (*Tnfa*, *Mcp1*), suggests a switch from the anti-inflammatory M2 to the pro-inflammatory M1 macrophage phenotype. Consistent with the increase in ER stress and inflammation, the protein levels of CHOP and of the p65 subunit of the pro-inflammatory transcription factor nuclear factor (NF)- κ B were increased in the liver of *Gdf15*-deficient mice (Fig. 3D). Hepatocellular death contributes to the progression of fatty liver to

nonalcoholic steatohepatitis (NASH), fibrosis and cirrhosis [24]. Of note, active caspase-6, a key mediator of inflammation-triggered hepatocyte death and liver injury [25], is a direct target of AMPK. Phosphorylation of caspase-6 at Ser²⁵⁷ by AMPK represses the cleavage and activation of this caspase [26]. In agreement with the reduction in phosphorylated AMPK levels, the levels of pro-caspase-6 phosphorylated at Ser²⁵⁷ were diminished in the livers of *Gdf15*^{-/-} mice, while the protein levels of cleaved caspase-3, considered a reliable marker for cells that are dying by apoptosis, were increased (Fig. 3E).

Since the TGF- β 1/SMAD3 pathway is a master regulator of fibrosis [27], we examined the levels of TGF- β 1 in the serum and liver. *Gdf15*^{-/-} mice displayed increased serum and hepatic levels of TGF- β 1 (Fig. 4A and B, respectively). Moreover, liver sections stained with Sirius red and Masson's trichrome revealed an important collagen deposition in the *Gdf15*^{-/-} mice, indicative of fibrosis development (Fig. 4C). Next, we examined the hepatic expression of several fibrogenic genes, mostly those encoding extracellular matrix proteins and tissue inhibitors of metalloproteinases (TIMPs). *Gdf15*^{-/-} mice showed increased hepatic mRNA levels of most of the evaluated SMAD3-target genes, such as *Col1a1*, *Serpine1* [which encodes the plasminogen activator inhibitor-1 (PAI-1) protein], *Timp3*, *Ctgf*, latent TGF- β binding protein 1 (*Ltbp1*) and *Acta2* [which encodes the α -smooth muscle actin (α -SMA) protein] (Fig. 4D), suggesting that the TGF- β 1/SMAD3 pathway was activated in mice deficient in *Gdf15*. Accordingly, the levels of phosphorylated SMAD3, which is activated by phosphorylation of the C-terminal serine residues, and of its targets PAI-1 and α -SMA were increased in the liver of *Gdf15*^{-/-} mice (Fig. 4E). Altogether, these findings indicate that *Gdf15* deficiency in mice drives liver fibrogenesis through the activation of the TGF- β 1/SMAD3 pathway.

3.3. Primary hepatocytes from *Gdf15*^{-/-} mice show increased levels of gluconeogenic and profibrotic genes, elevated glucose production and enhanced lipid accumulation

To confirm that the results observed in the liver were not influenced by the indirect action of *Gdf15* deletion in other organs, we isolated primary hepatocytes from WT and *Gdf15*^{-/-} mice. Primary hepatocytes from *Gdf15*^{-/-} mice showed increased expression of the gluconeogenic genes *Ppargc1a*, *G6pc1* and *Pck1* (Fig. 5A). Consistent with this, the protein levels of PEPCK and G6Pase (Fig. 5B) and the production of glucose (Fig. 5C) were higher compared to WT hepatocytes. Likewise, a reduction in phosphorylated AMPK was observed in primary hepatocytes deficient in *Gdf15* (Fig. 5D) that was accompanied by an increase in lipid accumulation (Fig. 5E). Finally, primary hepatocytes from *Gdf15*^{-/-} mice displayed elevated mRNA levels of *Tgfb* and the SMAD3-target genes *Serpine1*, *Acta2* and *Ctgf* (Fig. 5F). In line with these results, *Gdf15*^{-/-} hepatocytes also showed increased levels of phosphorylated SMAD3 and α -SMA (Fig. 5F). Collectively, these findings indicate that the increase in hepatocyte gluconeogenesis and fibrogenesis in *Gdf15*^{-/-} mice is not the result of the indirect action of other organs.

3.4. rGDF15 activates AMPK and reduces the levels of gluconeogenic and fibrotic markers in mouse primary hepatocytes and liver

Our findings suggest that *Gdf15* deficiency results in the activation of the TGF- β 1/SMAD3 pathway, which in turn attenuates AMPK phosphorylation, eventually leading to increased gluconeogenesis. In addition, the increased phosphorylation of SMAD3 promotes hepatic fibrosis. Next, we examined whether rGDF15 affected these pathways in mouse primary hepatocytes. Treatment with rGDF15 reduced PP2A levels and increased the phosphorylated levels of AMPK (Fig. 6A). In line with these results, rGDF15 caused a decrease in the accumulation of

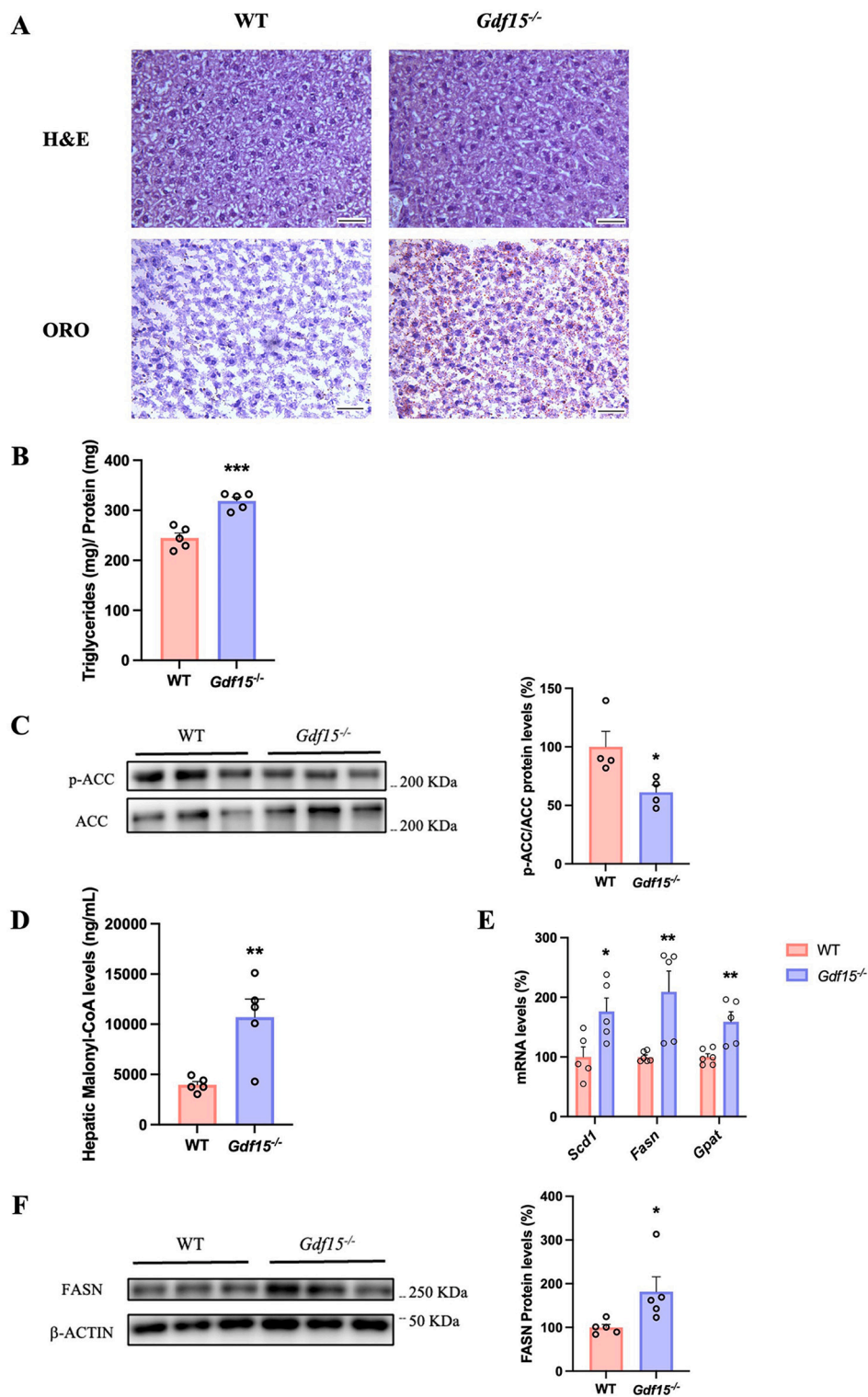


Fig. 2. *Gdf15*^{-/-} mice display increased hepatic steatosis.

(A) Representative images of liver sections and quantification of hematoxylin–eosin (H&E) and Oil Red O (ORO) staining in WT and *Gdf15*^{-/-} mice. Scale bar: 100 μm. n = 4 per group. (B) Hepatic triglyceride content. (C) Immunoblot analysis of total and phosphorylated ACC in the liver. n = 4 per group. (D) Hepatic malonyl-CoA levels in WT and *Gdf15*^{-/-} mice. (E) mRNA levels of *Scd1*, *Fasn* and *Gpat* in the liver. n = 5 per group. (F) Immunoblot analysis of FASN in the livers of WT and *Gdf15*^{-/-} mice. n = 5 per group. Data are presented as the mean ± SEM. Significant differences were established by Student’s t-test. *p < 0.05 and **p < 0.01 vs. WT. (For interpretation of the references to colour in this figure legend, the reader is referred to the web version of this article.)

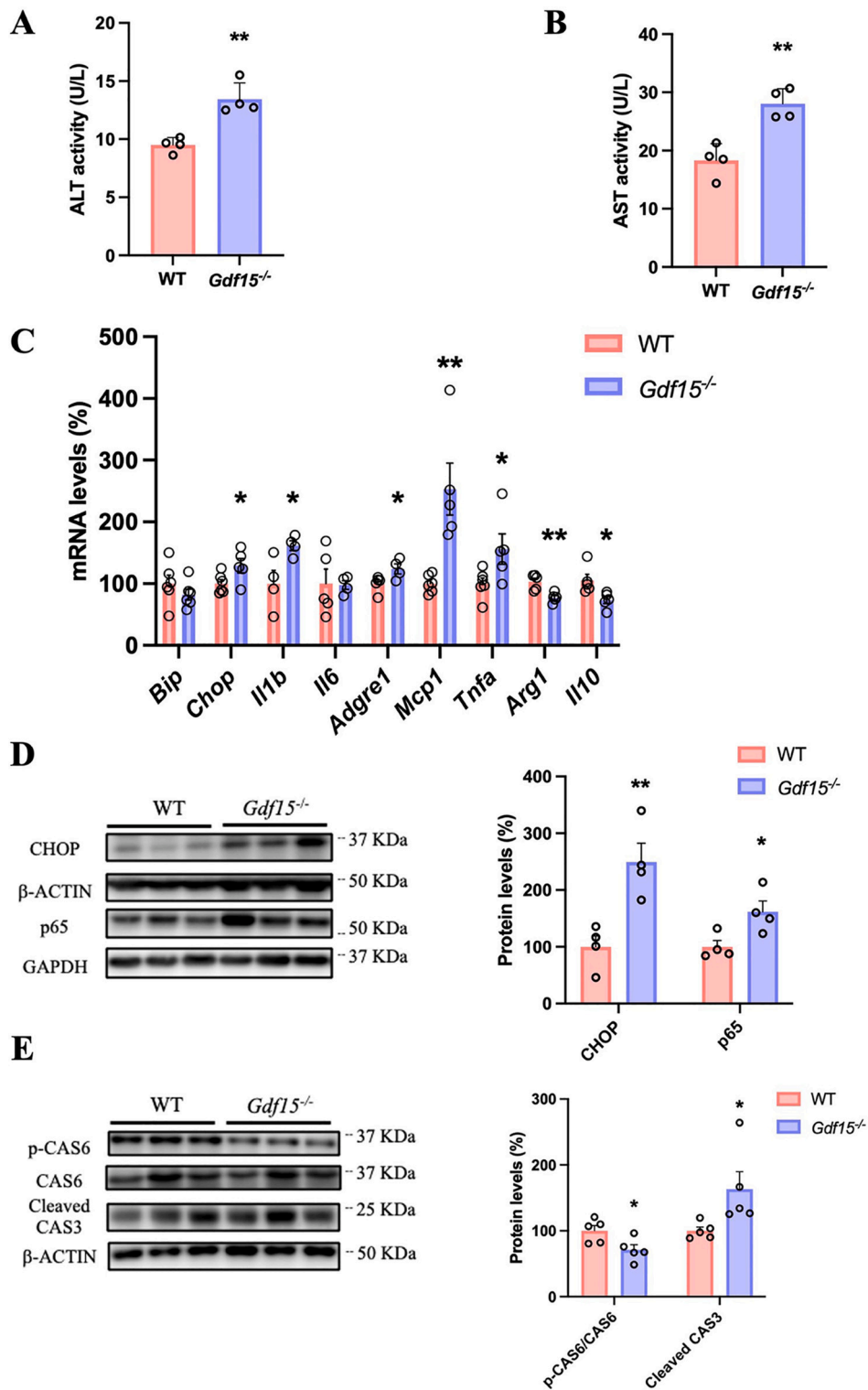


Fig. 3. *Gdf15*^{-/-} mice show liver damage, increased hepatic ER stress and apoptosis. Serum ALT (A) and AST (B) activities in WT and *Gdf15*^{-/-} mice. n = 4 per group. (C) mRNA levels of *BiP*, *Chop*, *Il1b*, *Il6*, *Adgre1*, *Mcp1*, *Tnfa*, *Arg1* and *Il10* in the liver of WT and *Gdf15*^{-/-} mice. n = 5 per group. (D) Immunoblot analysis of CHOP and the p65 subunit of NF- κ B in the liver of WT and *Gdf15*^{-/-} mice. n = 4 per group. (E) Immunoblot analysis of total (CAS6) and phosphorylated caspase-6 (p-CAS6) and cleaved caspase-3 (CAS3) in the liver of WT and *Gdf15*^{-/-} mice. n = 5 per group. Data are presented as the mean \pm SEM. Significant differences were established by Student's t-test. *p < 0.05 and **p < 0.01 vs. WT.

lipids in the presence or absence of palmitic acid (Fig. 6B). Likewise, the phosphorylated levels of CRCT2 and the levels of the gluconeogenic proteins PEPCK and G6Pase were reduced by rGDF15 (Fig. 6C). rGDF15 treatment also reduced the fibrogenic pathway, as demonstrated by the decrease in the phosphorylated levels of SMAD3 and PAI-1 protein levels

(Fig. 6D). These results confirm that the reductions in SMAD3 phosphorylation and PP2A levels caused by rGDF15 are accompanied by a subsequent increase in AMPK phosphorylation, which eventually leads to a decrease in the levels of the markers of gluconeogenesis and fibrosis. Moreover, these effects of rGDF15 were independent of GFRAL, since

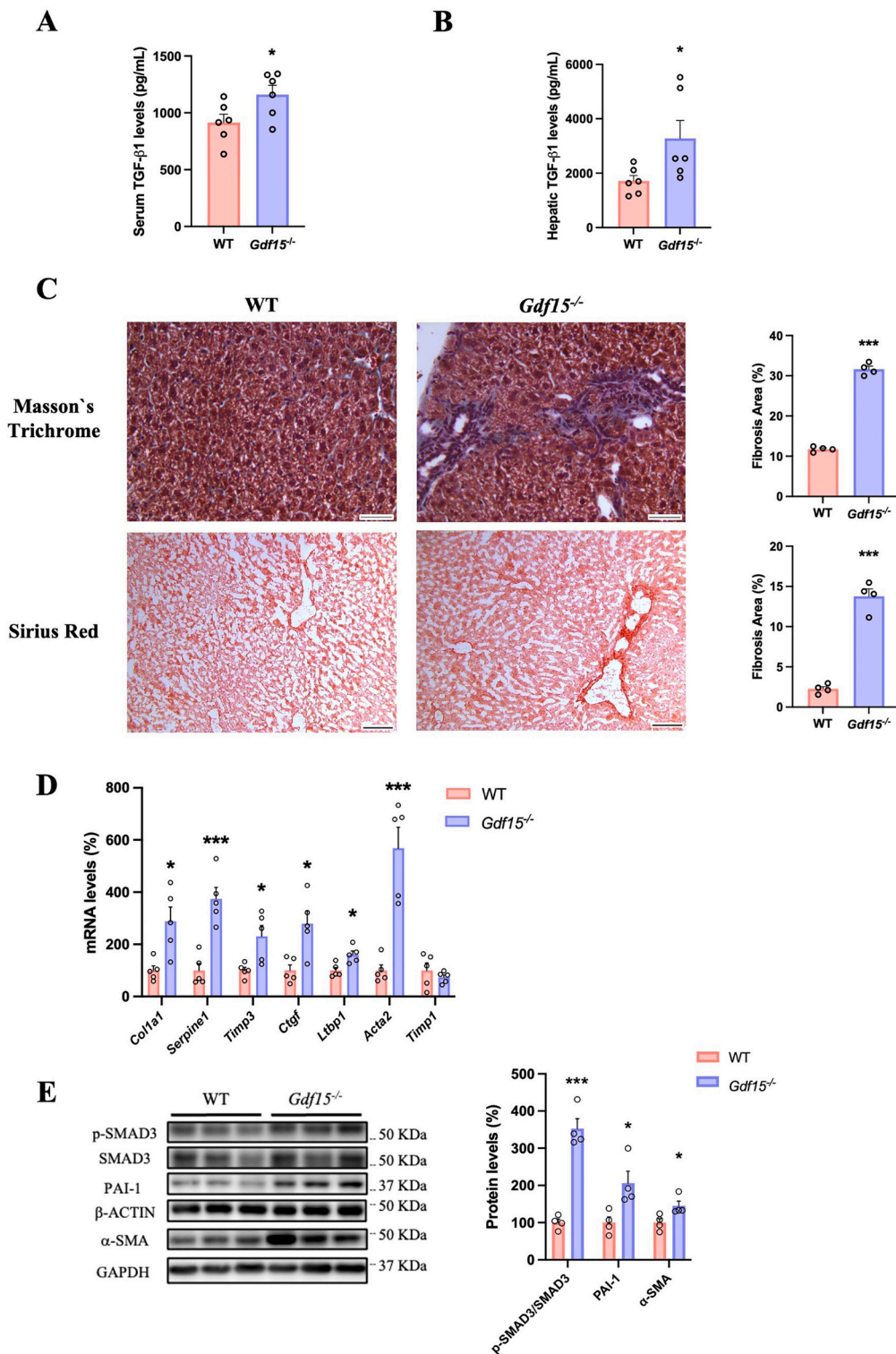


Fig. 4. *Gdf15*^{-/-} mice show increased hepatic fibrosis and activation of the TGF-β1/SMAD3 pathway. Serum (A) and hepatic (B) TGF-β1 levels in WT and *Gdf15*^{-/-} mice. *n* = 6 per group. (C) Representative images of liver sections and quantification of Masson's trichrome and Sirius red stainings in WT and *Gdf15*^{-/-} mice. Scale bar: 100 μm. *n* = 4 per group. (D) mRNA levels of *Col1a1*, *Serpine1*, *Timp3*, *Ctgf*, *Ltbp1*, *Acta2* and *Timp1* in the liver of WT and *Gdf15*^{-/-} mice. *n* = 5 per group. (E) Immunoblot analysis of total and phosphorylated SMAD3, PAI-1 and α-SMA in the liver of WT and *Gdf15*^{-/-} mice. *n* = 4 per group. Data are presented as the mean ± SEM. Significant differences were established by Student's t-test. **p* < 0.05 and ****p* < 0.001 vs. WT. (For interpretation of the references to colour in this figure legend, the reader is referred to the web version of this article.)

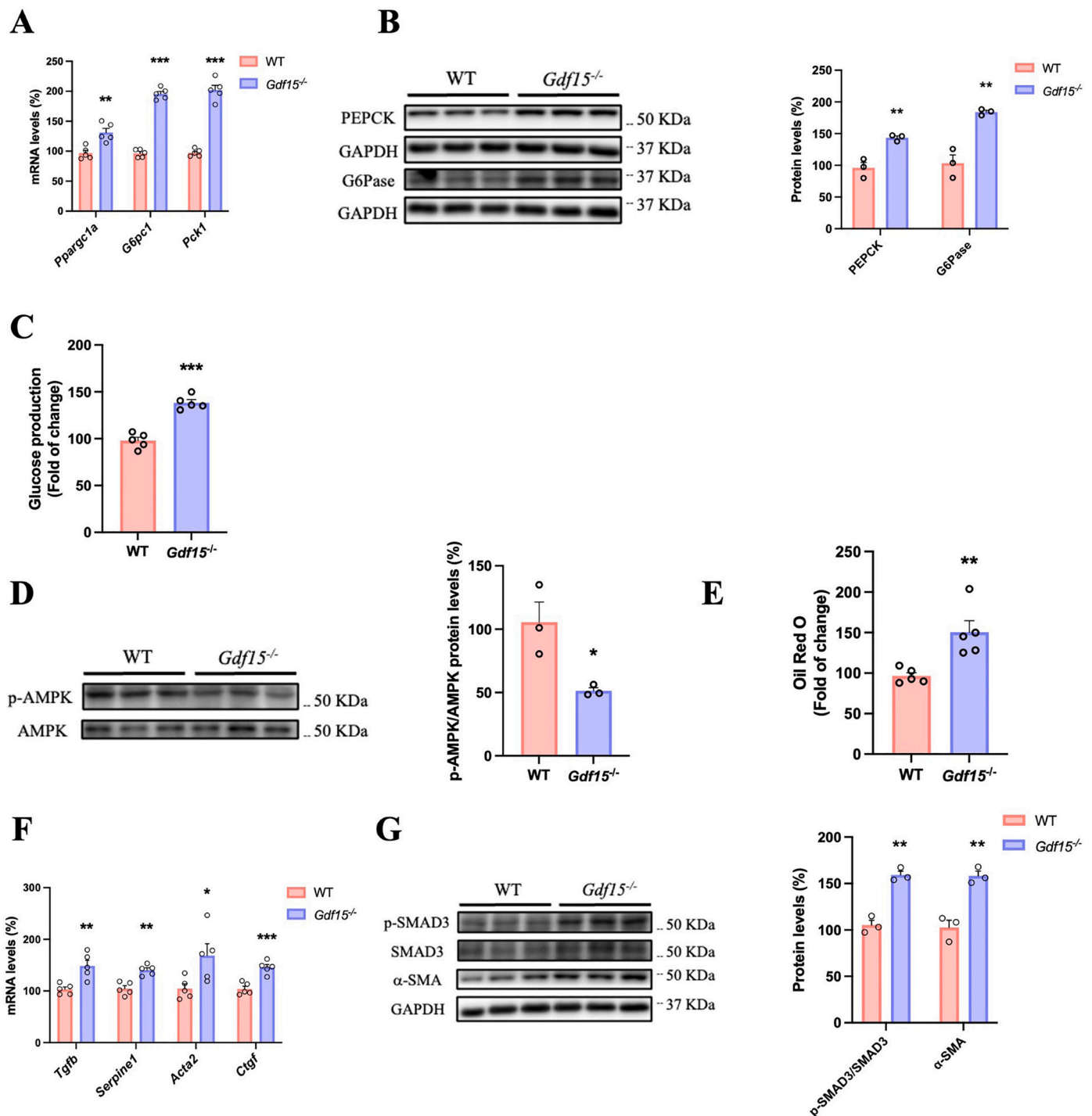


Fig. 5. Increased levels of gluconeogenic and profibrotic genes, elevated glucose production and lipid accumulation in mouse primary hepatocytes from *Gdf15*^{-/-} mice.

(A) mRNA levels of *Ppargc1a*, *G6pc1* and *Pck1* in primary hepatocytes from the livers of WT and *Gdf15*^{-/-} mice. n = 5 per group. (B) Immunoblot analysis of PEPCK and G6Pase. n = 3 per group. (C) Glucose production. n = 5 per group. (D) Immunoblot analysis of total and phosphorylated AMPK. n = 3 per group. (E) Lipid accumulation. (F) mRNA levels of *Tgfb*, *Serpine1*, *Acta2* and *Ctgf*. n = 5 per group. (G) Immunoblot analysis of total and phosphorylated SMAD3 and α -SMA. n = 3 per group. Data are presented as the mean \pm SEM. Significant differences were established by Student's t-test. *p \leq 0.05 and **p \leq 0.01 and ***p \leq 0.001 vs. WT primary hepatocytes.

mouse primary hepatocytes do not express this receptor [3].

We then examined if the effect of rGDF15 was also observed *in vivo*. Subcutaneous administration of a single dose of this cytokine to the mice reduced serum TGF- β 1 levels (Fig. 7A) and increased the phosphorylated levels of AMPK in the liver (Fig. 7B). This was accompanied by an increase in phosphorylated CRTC2 levels and a reduction in PP2A levels

(Fig. 7C). Administration of rGDF15 also reduced the protein levels of the gluconeogenic markers PEPCK and G6Pase (Fig. 7D). Likewise, rGDF15 treatment reduced the levels of phosphorylated SMAD3 and PAI-1 (Fig. 7E). Collectively, these findings, together with those obtained in the *Gdf15*^{-/-} mice, suggest that GDF15 attenuates the TGF- β 1/SMAD3 pathway resulting in the promotion of AMPK activation, and

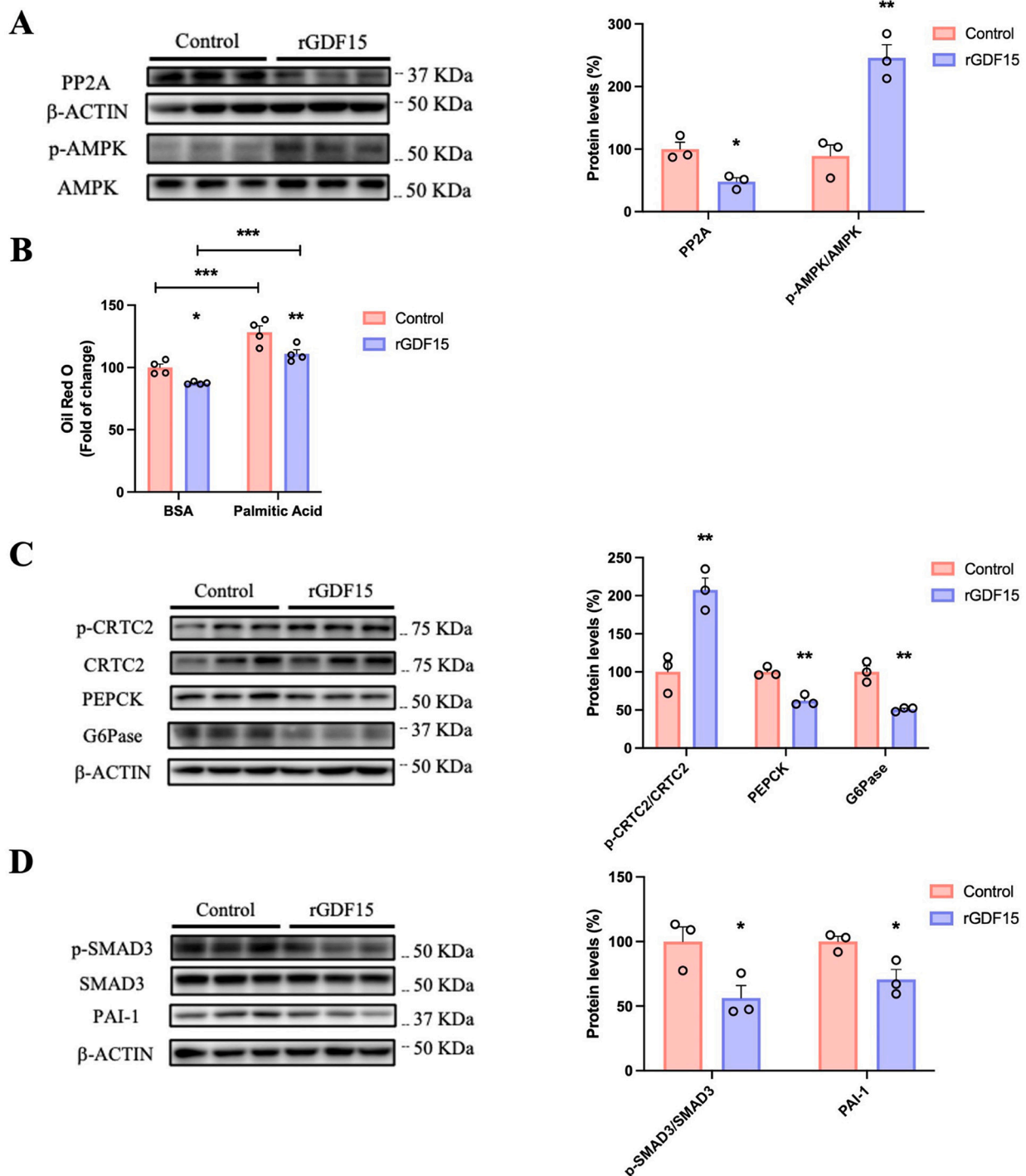


Fig. 6. rGDF15 activates AMPK and reduces the levels of gluconeogenic and fibrotic markers in mouse primary hepatocytes. (A) Immunoblot analysis of PP2A and total and phosphorylated AMPK in mouse primary hepatocytes in the absence (control) or presence of 100 ng/mL of rGDF15 for 24 h. n = 3 per group. (B) Lipid accumulation in mouse primary hepatocytes in the absence (control) or presence of fatty acid-free BSA or BSA conjugated with palmitic acid and 500 ng/mL of rGDF15 for 24 h. n = 4 per group. (C) Immunoblot analysis of total and phosphorylated CRTC2, PEPCK and G6Pase in mouse primary hepatocytes in the absence (control) or presence of 100 ng/mL of rGDF15 for 24 h. n = 3 per group. (D) Immunoblot analysis of total and phosphorylated SMAD3 and PAI-1 in mouse primary hepatocytes in the absence (control) or presence of 100 ng/mL of rGDF15 for 24 h. n = 3 per group. Data are presented as the mean ± SEM. Significant differences were established by Student's t-test. *p < 0.05 and **p < 0.01 vs. WT.

downregulation of gluconeogenesis and fibrosis.

3.5. Pharmacological inhibition of SMAD3 phosphorylation prevents the reduction in phosphorylated AMPK levels and the metabolic alterations in *Gdf15*^{-/-} mice

To demonstrate that SMAD3 activation in the *Gdf15*^{-/-} mice was responsible for the reduction in AMPK phosphorylation and for the

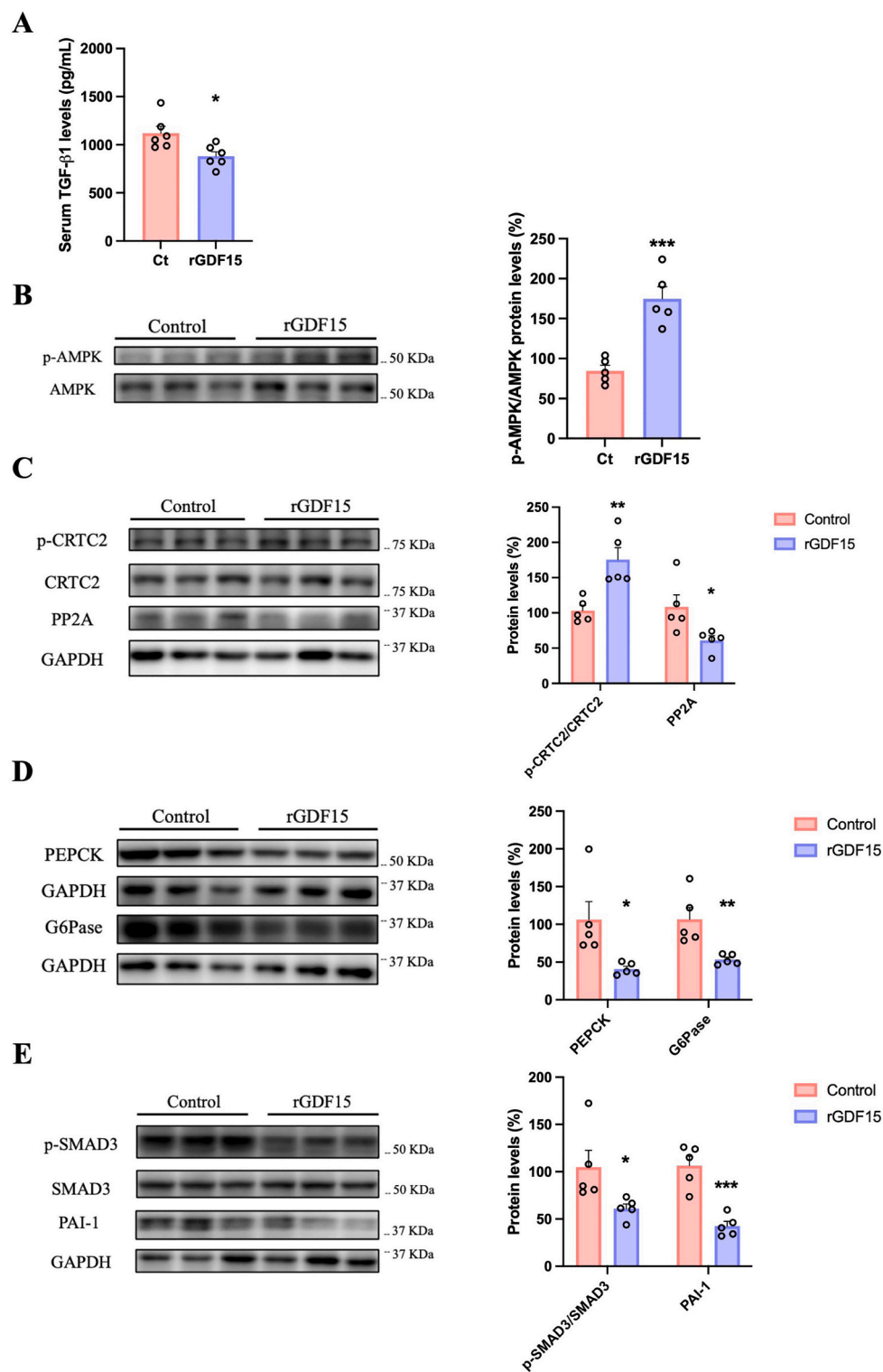


Fig. 7. rGDF15 activates AMPK and reduces the levels of hepatic gluconeogenic and fibrotic markers.

(A) Serum TGF-β1 levels in mice treated with saline or recombinant GDF15 (rGDF15). n = 6 per group. Immunoblot analysis of (B) total and phosphorylated AMPK, (C) total and phosphorylated CRTC2 and PP2A, (D) PEPCK and G6Pase, and (E) total and phosphorylated SMAD3 and PAI-1 in the liver of mice treated with saline or rGDF15. n = 5 per group. Data are presented as the mean ± SEM. Significant differences were established by Student's t-test. *p < 0.05, **p < 0.01 and ***p < 0.001 vs. WT.

metabolic alterations observed in these animals, we took advantage of the specific inhibitor of SMAD3 phosphorylation, SIS3 [16]. Incubation of human Huh-7 hepatic cells with SIS3 increased phosphorylated AMPK levels and reduced PP2A levels (Fig. 8A), suggesting that SMAD3 controls the activation of AMPK by regulating PP2A. Consistent with the

increase in phosphorylated AMPK levels, SIS3 treatment led to a reduction in the levels of the gluconeogenic proteins PEPCK and G6Pase (Fig. 8A). Regarding the fibrosis markers, SIS3 reduced phosphorylated SMAD3 levels and the protein levels of its targets PAI-1 and α-SMA (Fig. 8B). We next explored whether SIS3 administration rescued the

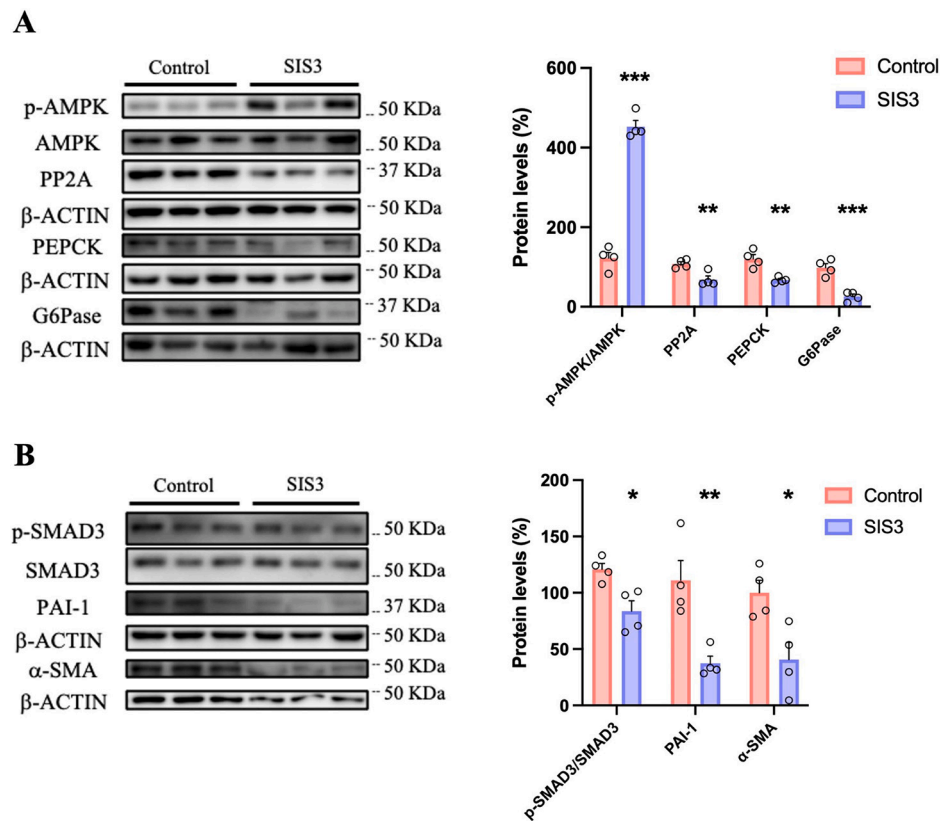


Fig. 8. The inhibitor of SMAD3 phosphorylation, SIS3, reduces PP2A levels and activates AMPK in human Huh-7 cells.

Immunoblot analysis of (A) total and phosphorylated AMPK, PP2A, PEPCK and G6Pase, and (B) total and phosphorylated SMAD3, PAI-1 and α -SMA in human Huh-7 cells in the absence (control) or presence of 10 μ M SIS3 for 24 h. n = 4 per group. Significant differences were established by Student's t-test. *p < 0.05, **p < 0.01 and ***p < 0.001 vs. WT.

metabolic alterations in the *Gdf15*^{-/-} mice. Remarkably, administration of SIS3 to the *Gdf15*-deficient mice ameliorated glucose intolerance (Fig. 9A-B) and attenuated hepatic lipid accumulation as demonstrated by quantification of the accumulation of triglycerides in the liver (Fig. 9C) and by H&E and ORO staining (Fig. 9D). Likewise, Masson's trichrome and Sirius red staining showed that SIS3 reduced fibrosis (Fig. 9E). In addition, SIS3 treatment restored hepatic phosphorylated AMPK levels, whereas the protein levels of PEPCK and PP2A were reduced (Fig. 9F). Treatment with SIS3 also reduced the levels of phosphorylated SMAD3, PAI-1 and α -SMA (Fig. 9G). No significant differences were observed in body weight (Supplementary Fig. 2A) or food intake (Supplementary Fig. 2B) between the WT and *Gdf15*^{-/-} mice receiving either vehicle or SIS3. Collectively, these findings confirmed that activation of SMAD3 contributed to the dysregulation of AMPK, gluconeogenesis and fibrosis in the *Gdf15*^{-/-} mice.

4. Discussion

AMPK is a central regulator of multiple metabolic pathways and the regulation of this kinase is of therapeutic interest in the treatment of insulin resistance, type 2 diabetes mellitus and NAFLD [20]. The previous discovery that *Gdf15*^{-/-} mice exhibited lower levels of phosphorylated AMPK [14] suggested that GDF15 regulates this cellular energy sensor. However, the mechanisms linking *Gdf15* deficiency to lower activity of AMPK have remained unknown. In this study, we provide a potential mechanism by which GDF15 regulates AMPK. According to our findings, *Gdf15* deficiency results in elevated serum TGF- β 1 levels and hepatic SMAD3 phosphorylation, which in turn augment the levels of PP2A, eventually reducing AMPK phosphorylation and thus, its activity (Fig. 10). These changes were observed in the absence

of variations in food intake and body weight between WT and *Gdf15*^{-/-} mice fed a control diet, which is consistent with previous studies reporting that these mice do not show an increase in food intake on a regular diet [28,29]. However, when challenged with a high-fat diet (HFD), *Gdf15*-null mice have been reported to increase food intake compared to WT mice [28,29]. In addition, the increase in phosphorylated SMAD3 levels in the *Gdf15*^{-/-} mice may promote the development of fibrosis, whereas the reduction in AMPK activity can ultimately result in hepatic steatosis and increased gluconeogenesis. Consistent with this, rGDF15 attenuates SMAD3 phosphorylation and reduces PP2A levels in mouse primary hepatocytes and the liver of mice, thereby activating AMPK, which leads to a reduction in the levels of the markers of fibrosis and gluconeogenesis. Moreover, the changes observed in the livers of *Gdf15*-null mice are not indirectly mediated by other organs since they were confirmed in primary hepatocytes obtained from these mice. Overall, these findings point to the inhibition of the TGF- β 1/SMAD3 pathway as a key regulator of the metabolic effects of GDF15.

SMAD3 is a critical intracellular mediator of TGF- β 1 signaling that is regulated through phosphorylation. In the canonical pathway, TGF- β 1 signals through the TGF- β type I and type II receptors that recruit and phosphorylate SMAD2 and SMAD3 [30], with SMAD3 being the preferred downstream transcription factor for the TGF- β receptors. In our study, TGF- β 1 serum levels were increased in the *Gdf15*^{-/-} mice, suggesting that the activation of SMAD3 involves TGF- β type I and type II receptors. A previous study reported that pro-GDF15 accumulates in the nucleus, where it attenuates TGF- β 1-induced signaling by interrupting the DNA binding capacity of the SMAD complex [31]. The authors of that study examined the effects of GDF15 on SMAD2 phosphorylation in cancer cells and found no changes, whereas SMAD3 phosphorylation was not evaluated. In our study, phosphorylated

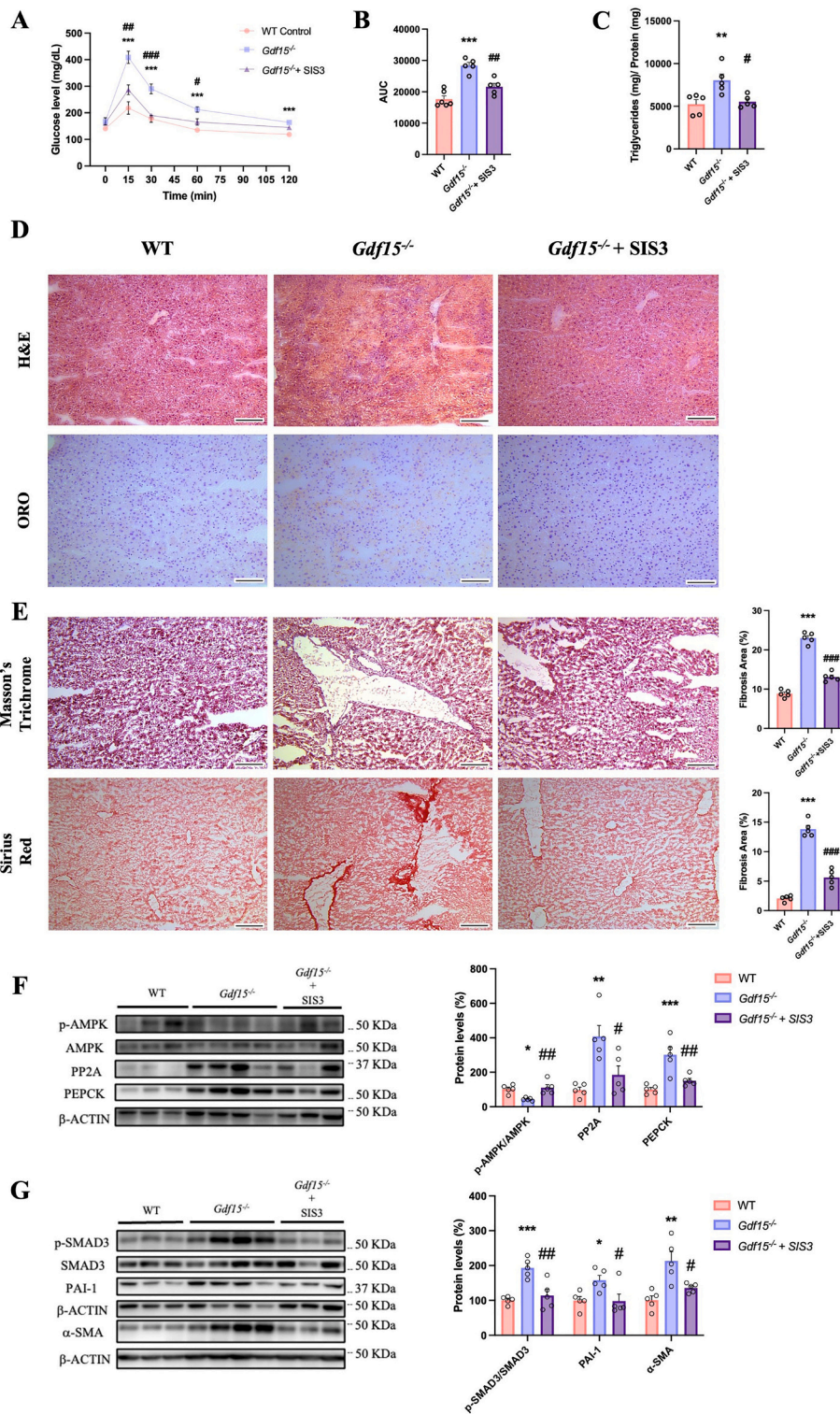


Fig. 9. Pharmacological inhibition of SMAD3 prevents phosphorylated AMPK reduction, metabolic alterations and fibrosis in *Gdf15*^{-/-} mice. (A) Glucose tolerance test (GTT) and (B) area under the curve (AUC) in WT and *Gdf15*^{-/-} mice treated with vehicle or SIS3. n = 5 per group. (C) Hepatic triglyceride content. (D) Representative images of liver sections and the quantification of hematoxylin-eosin (H&E) and Oil Red O (ORO) staining in WT and *Gdf15*^{-/-} mice treated with vehicle or SIS3. Scale bar: 100 μm. n = 5 per group. (E) Representative images of liver sections and the quantification of Masson's trichrome and Sirius red staining in WT and *Gdf15*^{-/-} mice treated with vehicle or SIS3. Scale bar: 100 μm. n = 5 per group. Immunoblot analysis of (F) total and phosphorylated AMPK, PP2A and PEPCK and (G) total and phosphorylated SMAD3, PAI-1 and α-SMA in WT and *Gdf15*^{-/-} mice treated with vehicle or SIS3. Data are presented as the mean ± SEM. n = 5 per group. Significant differences were established by Student's t-test or one-way ANOVA with Tukey's post-hoc test. *p < 0.05, **p < 0.01 and ***p < 0.001 vs. WT. #p < 0.05, ##p < 0.01 and ###p < 0.001 vs. *Gdf15*^{-/-} mice treated with vehicle. (For interpretation of the references to colour in this figure legend, the reader is referred to the web version of this article.)

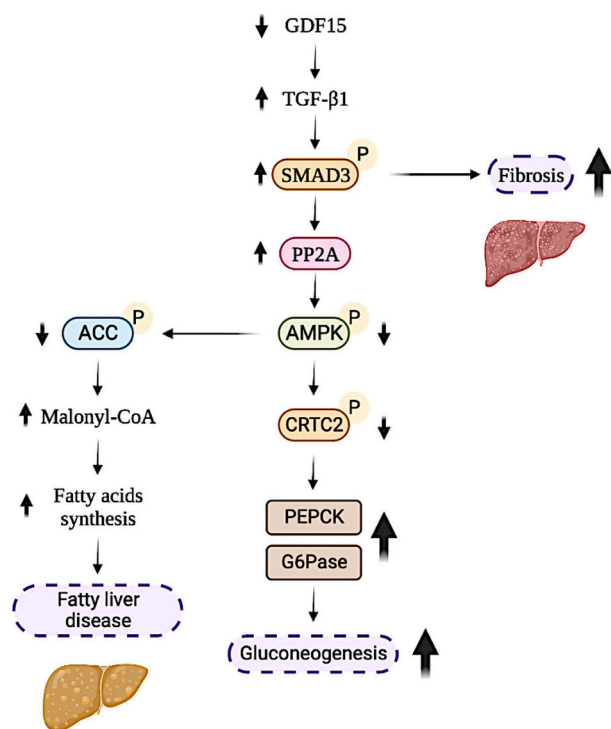


Fig. 10. Proposed mechanistic model for the hepatic effects of *Gdf15* deficiency on fibrosis, gluconeogenesis and fatty liver via the TGF- β 1-SMAD3 pathway.

SMAD3 levels were increased in the liver of *Gdf15*^{-/-} mice, while rGDF15 treatment reduced its phosphorylation in mouse primary hepatocytes and the liver of mice. Since serum TGF- β 1 levels were increased in the *Gdf15*^{-/-} mice and given that rGDF15 administration reduced circulating TGF- β 1 in these mice, our findings suggest that GDF15 regulates the levels of this cytokine. Previous studies have reported that AMPK activation reduces TGF- β 1 expression and protein levels [32], suggesting that the reduction in AMPK activity in the *Gdf15*^{-/-} mice might be responsible for the increase in TGF- β 1 levels. Remarkably, plasma TGF- β 1 levels are increased in patients with type 2 diabetes compared to healthy subjects, while metformin, an antidiabetic drug that activates AMPK, reduces its levels when compared to other glucose-lowering drugs [32]. Since metformin increases GDF15 levels in humans and mice [1,19,33,34], these findings seem to reinforce a relationship between AMPK, GDF15 and the TGF- β 1/SMAD3 pathway. Further studies are needed to assess whether GDF15 is required for the reduction of TGF- β 1 levels following metformin treatment.

We also report that the reduced phosphorylated AMPK levels caused by the increased SMAD3 activation in the liver of *Gdf15*^{-/-} mice contribute to increased steatosis and gluconeogenesis. Previous studies have reported that GDF15 binds to a receptor on hepatocytes that is yet to be identified, preventing excess lipid accumulation [35,36]. These effects are caused by a GDF15-mediated upregulation of PPAR α , a transcription factor that promotes an increase in fatty acid oxidation. Our findings now add a new mechanism by which GDF15 prevents lipid accumulation, since its deficiency reduces AMPK activity, ultimately leading to increases in malonyl-CoA levels and in the expression of genes involved in fatty acid synthesis. Moreover, *Gdf15* deficiency promotes gluconeogenesis via a reduction in AMPK activity because this kinase inhibits gluconeogenesis by phosphorylating CRTC2, which in turn upregulates the levels of the gluconeogenic enzymes PEPCK and G6Pase [21,22]. Although IL-6 has been reported to play an important role in hepatic gluconeogenesis [37], we did not observe changes in the hepatic expression of this cytokine in *Gdf15*^{-/-} mice, which is consistent with a previous study reporting that stress-inducible IL-6 that increases hyperglycemia is produced by brown adipose tissue [38]. Collectively,

these findings support a role for SMAD3 in regulating gluconeogenesis in the liver, which is in line with previous studies [39].

GDF15 has been reported to ameliorate fibrosis. In fact, rGDF15 or the genetic overexpression of this cytokine improves inflammatory and fibrotic phenotypes [40,41]. Similarly, *Gdf15*^{-/-} mice have been previously reported to exhibit aggravated hepatic inflammation and fibrotic features after exposure to a NASH diet, alcohol liquid diet or CCl₄ [40,41]. Several studies have confirmed these beneficial effects of GDF15 on fibrosis [35], whereas others have reported that GDF15 acts as a pro-fibrotic factor in mouse liver fibrosis progression [42]. In agreement with previous studies [41], our findings demonstrate that GDF15 deficiency promotes fibrosis. Consistent with this, we show that in the absence of GDF15, SMAD3, a key mediator of the fibrotic response, is activated in the liver, whereas treatment with rGDF15 has the opposite effect in mouse primary hepatocytes and the liver of mice. Likewise, the reduction of AMPK activity in the *Gdf15*^{-/-} mice can also exacerbate fibrosis, in line with the observations that this kinase ameliorates insulin resistance and directly suppresses inflammation and fibrogenesis in mice with NASH [43].

The present study also demonstrated that the effects of GDF15 on SMAD3 and AMPK and the changes in the protein markers of gluconeogenesis and fibrosis in mouse primary hepatocytes are independent of GFRAL, since these cells do not express this receptor [3]. These findings suggest the presence of a receptor, which has not been discovered yet, mediating the peripheral effects of GDF15 in hepatocytes. In fact, previous studies have supported the presence of these peripheral effects of GDF15 that do not involve GFRAL [12–14,19].

Altogether, the findings of this study demonstrate that GDF15 attenuates the TGF- β 1/SMAD3 pathway, which in turn results in AMPK activation. These effects result in a reduction in gluconeogenesis, the main contributor to hyperglycemia in the fasting state in patients with type 2 diabetes mellitus due to insulin resistance, and fibrosis.

4.1. Limitations of the study

The findings of this study point to an effect of GDF15 on AMPK that is independent of central GFRAL, since it was observed in mouse primary hepatocytes. In addition, rGDF15 administration increased AMPK phosphorylation in the liver of fasted mice, excluding the possibility that this effect might be related to GFRAL-mediated changes in food intake. However, studies using neutralizing antibodies against GFRAL or GFRAL-knockout mice are needed to dismiss this possibility. Another limitation of this study is that it does not provide the identity of the peripheral receptor mediating the effects of GDF15 on hepatocytes. The search for this peripheral receptor is challenging since GFRAL was robustly identified as the receptor mediating the effects of GDF15 [3–5]. Several membrane-expressed proteins have been suggested to be additional GDF15-binding partners, although they bind GDF15 with lower affinity [3,4]. More recently, it has been reported that GDF15 acts in T cells through CD48, which is mainly expressed in lymphoid cells [13]. Likewise, the anti-inflammatory effects of colchicine have been reported to be mediated by GDF15 through an unidentified receptor on myeloid cells that requires further characterization [12]. Furthermore, we cannot exclude the involvement of GDF15-mediated nuclear effects, since it has been reported that this cytokine controls transcription [31]. Future studies are needed to uncover the receptor/s involved in the peripheral effects of GDF15.

Supplementary data to this article can be found online at <https://doi.org/10.1016/j.metabol.2023.155772>.

Funding sources

This study was partly supported by the grants PID2021-122116OB-I00 (M.V.-C.) and PID2021-122766OB-I00 (A.M.V.) from MCIN/AEI/10.13039/501100011033 and “ERDF, A Way of Making Europe”. CIBER de Diabetes y Enfermedades Metabólicas Asociadas (CIBERDEM) is a

Carlos III Health Institute project. Support was also received from the CERCA Programme/Generalitat de Catalunya. Meijian Zhang was supported by a grant from the China Scholarship Council (CSC) (202007565030).

CRedit authorship contribution statement

Javier Jurado-Aguilar: Formal analysis, Investigation, Methodology. **Emma Barroso:** Data curation, Formal analysis, Investigation. **Maribel Bernard:** Investigation. **Meijian Zhang:** Investigation. **Mona Peyman:** Investigation. **Patricia Rada:** Investigation, Methodology. **Ángela M. Valverde:** Investigation, Methodology. **Walter Wahli:** Investigation, Writing – review & editing. **Xavier Palomer:** Investigation, Writing – review & editing. **Manuel Vázquez-Carrera:** Conceptualization, Formal analysis, Funding acquisition, Investigation, Project administration, Writing – original draft.

Declaration of competing interest

The authors have no conflicts of interest to declare.

Data availability

The study data are available upon request.

Acknowledgements

We are indebted to the Biobank core facility of the Institut d'Investigacions Biomèdiques August Pi i Sunyer (IDIBAPS) for the technical help. We would like to thank the Language Services of the University of Barcelona for revising the manuscript.

References

- [1] Aguilar-Recarte D, Barroso E, Palomer X, Wahli W, Vazquez-Carrera M. Knocking on GDF15's door for the treatment of type 2 diabetes mellitus. *Trends Endocrinol Metab* 2022;33:741–54. <https://doi.org/10.1016/j.tem.2022.08.004>.
- [2] Emmerson PJ, Wang F, Du Y, Liu Q, Pickard RT, Gonciarz MD, et al. The metabolic effects of GDF15 are mediated by the orphan receptor GFRAL. *Nat Med* 2017;23:1215–9. <https://doi.org/10.1038/nm.4393>.
- [3] Mulligan SE, Lin-Schmidt X, Chin CN, Chavez JA, Furman JL, Armstrong AA, et al. GFRAL is the receptor for GDF15 and the ligand promotes weight loss in mice and nonhuman primates. *Nat Med* 2017;23:1150–7. <https://doi.org/10.1038/nm.4392>.
- [4] Hsu JY, Crawley S, Chen M, Ayupova DA, Lindhout DA, Higbee J, et al. Non-homeostatic body weight regulation through a brainstem-restricted receptor for GDF15. *Nature* 2017;550:255–9. <https://doi.org/10.1038/nature24042>.
- [5] Yang L, Chang CC, Sun Z, Madsen D, Zhu H, Padkjaer SB, et al. GFRAL is the receptor for GDF15 and is required for the anti-obesity effects of the ligand. *Nat Med* 2017;23:1158–66. <https://doi.org/10.1038/nm.4394>.
- [6] Johnen H, Lin S, Kuffner T, Brown DA, Tsai VW, Bauskin AR, et al. Tumor-induced anorexia and weight loss are mediated by the TGF-beta superfamily cytokine MIC-1. *Nat Med* 2007;13:1333–40. <https://doi.org/10.1038/nm1677>.
- [7] Wang X, Chrysovergis K, Kosak J, Eling TE. Lower NLRP3 inflammasome activity in NAG-1 transgenic mice is linked to a resistance to obesity and increased insulin sensitivity. *Obesity (Silver Spring)* 2014;22:1256–63. <https://doi.org/10.1002/oby.20638>.
- [8] Chrysovergis K, Wang X, Kosak J, Lee SH, Kim JS, Foley JF, et al. NAG-1/GDF-15 prevents obesity by increasing thermogenesis, lipolysis and oxidative metabolism. *Int J Obes (Lond)* 2014;38:1555–64. <https://doi.org/10.1038/ijo.2014.27>.
- [9] Macia L, Tsai VW, Nguyen AD, Johnen H, Kuffner T, Shi YC, et al. Macrophage inhibitory cytokine 1 (MIC-1/GDF15) decreases food intake, body weight and improves glucose tolerance in mice on normal & obesogenic diets. *PLoS One* 2012;7:e34868. <https://doi.org/10.1371/journal.pone.0034868>.
- [10] Patel S, Alvarez-Guaita A, Melvin A, Rimmington D, Dattilo A, Miedzybrodzka EL, et al. GDF15 provides an endocrine signal of nutritional stress in mice and humans. *Cell Metab* 2019;29(707–718):e8. <https://doi.org/10.1016/j.cmet.2018.12.016>.
- [11] Chow CFW, Guo X, Asthana P, Zhang S, Wong SKK, Fallah S, et al. Body weight regulation via MT1-MMP-mediated cleavage of GFRAL. *Nat Metab* 2022;4:203–12. <https://doi.org/10.1038/s42255-022-00529-5>.
- [12] Weng JH, Koch PD, Luan HH, Tu HC, Shimada K, Ngan I, et al. Colchicine acts selectively in the liver to induce hepatokines that inhibit myeloid cell activation. *Nat Metab* 2021;3:513–22. <https://doi.org/10.1038/s42255-021-00366-y>.
- [13] Wang Z, He L, Li W, Xu C, Zhang J, Wang D, et al. GDF15 induces immunosuppression via CD48 on regulatory T cells in hepatocellular carcinoma. *J Immunother Cancer* 2021;9. <https://doi.org/10.1136/jitc-2021-002787>.
- [14] Aguilar-Recarte D, Barroso E, Guma A, Pizarro-Delgado J, Pena L, Ruat M, et al. GDF15 mediates the metabolic effects of PPARbeta/delta by activating AMPK. *Cell Rep* 2021;36:109501. <https://doi.org/10.1016/j.celrep.2021.109501>.
- [15] Hsiao EC, Koniaris LG, Zimmers-Koniaris T, Sebald SM, Huynh TV, Lee SJ. Characterization of growth-differentiation factor 15, a transforming growth factor beta superfamily member induced following liver injury. *Mol Cell Biol* 2000;20:3742–51. <https://doi.org/10.1128/MCB.20.10.3742-3751.2000>.
- [16] Ji X, Wang H, Wu Z, Zhong X, Zhu M, Zhang Y, et al. Specific inhibitor of Smad3 (SIS3) attenuates fibrosis, apoptosis, and inflammation in unilateral ureteral obstruction kidneys by inhibition of transforming growth factor beta (TGF-beta)/Smad3 signaling. *Med Sci Monit* 2018;24:1633–41. <https://doi.org/10.12659/msm.909236>.
- [17] Bligh EG, Dyer WJ. A rapid method of total lipid extraction and purification. *Can J Biochem Physiol* 1959;37:911–7. <https://doi.org/10.1139/o59-099>.
- [18] Benveniste R, Danoff TM, Illekis J, Craig HR. Epidermal growth factor receptor numbers in male and female mouse primary hepatocyte cultures. *Cell Biochem Funct* 1988;6:231–5. <https://doi.org/10.1002/cbf.290060403>.
- [19] Aguilar-Recarte D, Barroso E, Zhang M, Rada P, Pizarro-Delgado J, Pena L, et al. A positive feedback loop between AMPK and GDF15 promotes metformin antidiabetic effects. *Pharmacol Res* 2022;187:106578. <https://doi.org/10.1016/j.phrs.2022.106578>.
- [20] Lin SC, Hardie DG. AMPK: sensing glucose as well as cellular energy status. *Cell Metab* 2018;27:299–313. <https://doi.org/10.1016/j.cmet.2017.10.009>.
- [21] Miinalainen IJ, Schmitz W, Huotari A, Autio KJ, Soininen R, Loren Ver, et al. Mitochondrial 2,4-dienoyl-CoA reductase deficiency in mice results in severe hypoglycemia with stress intolerance and unimpaired ketogenesis. *PLoS Genet* 2009;5:e1000543. <https://doi.org/10.1371/journal.pgen.1000543>.
- [22] Sugden MC, Caton PW, Holness MJ. PPAR control: it's SIRTainly as easy as PGC. *J Endocrinol* 2010;204:93–104. <https://doi.org/10.1677/JOE-09-0359>.
- [23] Kropski JA, Blackwell TS. Endoplasmic reticulum stress in the pathogenesis of fibrotic disease. *J Clin Invest* 2018;128:64–73. <https://doi.org/10.1172/JCI93560>.
- [24] Luedde T, Kaplowitz N, Schwabe RF. Cell death and cell death responses in liver disease: mechanisms and clinical relevance. *Gastroenterology* 2014;147(765–783):e4. <https://doi.org/10.1053/j.gastro.2014.07.018>.
- [25] McIlwain DR, Berger T, Mak TW. Caspase functions in cell death and disease. *Cold Spring Harb Perspect Biol* 2013;5:a008656. <https://doi.org/10.1101/cshperspect.a008656>.
- [26] Zhao P, Sun X, Chaggaan C, Liao Z, In Wong K, He F, et al. An AMPK-caspase-6 axis controls liver damage in nonalcoholic steatohepatitis. *Science* 2020;367:652–60. <https://doi.org/10.1126/science.aay0542>.
- [27] Inagaki Y, Okazaki I. Emerging insights into transforming growth factor beta Smad signal in hepatic fibrogenesis. *Gut* 2007;56:284–92. <https://doi.org/10.1136/gut.2005.088690>.
- [28] Tran T, Yang J, Gardner J, Xiong Y. GDF15 deficiency promotes high fat diet-induced obesity in mice. *PLoS One* 2018;13:e0201584. <https://doi.org/10.1371/journal.pone.0201584>.
- [29] Wang D, Day EA, Townsend LK, Djordjevic D, Jorgensen SB, Steinberg GR. GDF15: emerging biology and therapeutic applications for obesity and cardiometabolic disease. *Nat Rev Endocrinol* 2021;17:592–607. <https://doi.org/10.1038/s41574-021-00529-7>.
- [30] Derynck R, Budi EH. Specificity, versatility, and control of TGF-beta family signaling. *Sci Signal* 2019;12. <https://doi.org/10.1126/scisignal.aav5183>.
- [31] Min KW, Liggett JL, Silva G, Wu WW, Wang R, Shen RF, et al. NAG-1/GDF15 accumulates in the nucleus and modulates transcriptional regulation of the Smad pathway. *Oncogene* 2016;35:377–88. <https://doi.org/10.1038/ncr.2015.95>.
- [32] Zou J, Li C, Jiang S, Luo L, Yan X, Huang D, et al. AMPK inhibits Smad3-mediated autoinduction of TGF-beta1 in gastric cancer cells. *J Cell Mol Med* 2021;25:2806–15. <https://doi.org/10.1111/jcmm.16308>.
- [33] Coll AP, Chen M, Taskar P, Rimmington D, Patel S, Tadross JA, et al. GDF15 mediates the effects of metformin on body weight and energy balance. *Nature* 2020;578:444–8. <https://doi.org/10.1038/s41586-019-1911-y>.
- [34] Day EA, Ford RJ, Smith BK, Mohammadi-Shemirani P, Morrow MR, Gutgesell RM, et al. Metformin-induced increases in GDF15 are important for suppressing appetite and promoting weight loss. *Nat Metab* 2019;1:1202–8. <https://doi.org/10.1038/s42255-019-0146-4>.
- [35] Zhang Z, Xu X, Tian W, Jiang R, Lu Y, Sun Q, et al. ARR1B1 inhibits non-alcoholic steatohepatitis progression by promoting GDF15 maturation. *J Hepatol* 2020;72:976–89. <https://doi.org/10.1016/j.jhep.2019.12.004>.
- [36] Abe H, Schuppman D. beta-arrestin: Dr Jekyll and Mr Hyde in NASH and fibrosis. *J Hepatol* 2020;72:813–5. <https://doi.org/10.1016/j.jhep.2020.01.016>.
- [37] Schmidt-Arras D, Rose-John S. IL-6 pathway in the liver: from physiopathology to therapy. *J Hepatol* 2016;64:1403–15. <https://doi.org/10.1016/j.jhep.2016.02.004>.
- [38] Qing H, Desrocheaux R, Israni-Winger K, Mineur YS, Fogelman N, Zhang C, et al. Origin and function of stress-induced IL-6 in murine models. *Cell* 2020;182:1660. <https://doi.org/10.1016/j.cell.2020.08.044>.
- [39] Yadav H, Devalaraja S, Chung ST, Rane SG. TGF-beta1/Smad3 pathway targets PP2A-AMPK-FoxO1 signaling to regulate hepatic gluconeogenesis. *J Biol Chem* 2017;292:3420–32. <https://doi.org/10.1074/jbc.M116.764910>.
- [40] Kim KH, Kim SH, Han DH, Jo YS, Lee YH, Lee MS. Growth differentiation factor 15 ameliorates nonalcoholic steatohepatitis and related metabolic disorders in mice. *Sci Rep* 2018;8:6789. <https://doi.org/10.1038/s41598-018-25098-0>.

- [41] Chung HK, Kim JT, Kim HW, Kwon M, Kim SY, Shong M, et al. GDF15 deficiency exacerbates chronic alcohol- and carbon tetrachloride-induced liver injury. *Sci Rep* 2017;7:17238. <https://doi.org/10.1038/s41598-017-17574-w>.
- [42] Qi P, Ma MZ, Kuai JH. Identification of growth differentiation factor 15 as a pro-fibrotic factor in mouse liver fibrosis progression. *Int J Exp Pathol* 2021;102:148–56. <https://doi.org/10.1111/iep.12398>.
- [43] Gluais-Dagorn P, Foretz M, Steinberg GR, Batchuluun B, Zawistowska-Deniziak A, Lambooj JM, et al. Direct AMPK activation corrects NASH in rodents through metabolic effects and direct action on inflammation and Fibrogenesis. *Hepatol Commun* 2022;6:101–19. <https://doi.org/10.1002/hep4.1799>.